International Journal of Technology 11(7)1309-1318 (2020)
Received July 2020 / Revised November 2020 / Accepted December 2020

International Journal of Technology

http://ijtech.eng.ui.ac.id

Synthesis of Schiff Base Encapsulated ZnS Nanoparticles: Characterization and Antibacterial Screening

Muhammad Saiful Omar[2*], Muhammad Nafis M. N. M. Sanif[1], Nur Halilatul Sadiqin Omar Ali[1], Malai Haniti Sheikh Abdul Hamid[1], Hussein Taha[2], Abdul Hanif Mahadi[3], Ying Woan Soon[4], Zainab Ngaini[5], Mohd Yameany H. Rosli[6], Anwar Usman[1]

[1]*Chemical Sciences, Faculty of Science, Universiti Brunei Darussalam, Jalan Tungku Link, Gadong BE1410, Brunei Darussalam*
[2]*Environmental and Life Sciences, Faculty of Science, Universiti Brunei Darussalam, Jalan Tungku Link, Gadong BE1410, Brunei Darussalam*
[3]*Centre for Advanced Material and Energy Sciences, Universiti Brunei Darussalam, Jalan Tungku Link, Gadong BE1410, Brunei Darussalam*
[4]*Applied Physics, Faculty of Science, Universiti Brunei Darussalam, Jalan Tungku Link, Gadong BE1410, Brunei Darussalam*
[5]*Faculty of Resource Science and Technology, Universiti Malaysia Sarawak, 94300 Kota Samarahan, Sarawak, Malaysia*
[6]*Geosciences, Faculty of Science, Universiti Brunei Darussalam, Jalan Tungku Link, Gadong BE1410, Brunei Darussalam*

Abstract. In this study, Schiff bases containing salicylaldehyde moiety (namely salicylaldehyde 2-methyl-3-thiosemicarbazone and salicylaldehyde triazole) were synthesized using the conventional refluxing method. The Schiff bases were utilized in the encapsulation of ZnS nanoparticles using the co-precipitation method. The nanoparticles were characterized using FTIR, UV-visible absorption spectroscopy, scanning electron microscopy, and energy dispersive X-ray analysis. X-ray diffraction analyses suggest that the Schiff base encapsulated ZnS particles form the cubic crystal phase of ZnS, with the average crystallite sizes being approximately between 56 and 60 nm. The interaction between the Schiff bases and ZnS was also evaluated by photoluminescence spectroscopy. The antibacterial activities of the Schiff base encapsulated ZnS nanoparticles were screened against four different gram-positive and gram-negative bacterial strains (*i.e. Escherichia coli, Bacillus subtilis, Pseudomonas aeruginosa,* and *Staphylococcus aureus)* using the agar diffusion method. The antibacterial activities of the nanoparticles were compared with those of their respective Schiff bases. Although in the current study the Schiff base encapsulated ZnS nanoparticles were found to be inactive against those bacteria, they could be applicable as multifunctional materials for fluorescence probes, photocatalysts, and other biological applications.

Keywords: Antibacterial activity; Co-precipitation; Encapsulation; Schiff base; ZnS nanoparticles

1. Introduction

Semiconductor materials of groups II–IV are commonly used due to their attractive electronic and optical properties (Keskin et al., 2019). These types of semiconductor materials are used in a wide range of applications due to their broad absorption range,

*Corresponding author's email: poll1709@hotmail.com, Tel.: +6737254597
doi: 10.14716/ijtech.v11i7.4486

tunable bandgap, spectral purity, and photochemical stability (Mansur et al., 1999; Carrillo-Carrión et al., 2009; Mansur, 2010; Wei et al., 2016).

An interesting feature of semiconductor materials is that they can be prepared in a few nanometer-sized crystals, which have physical and chemical properties that are different from those of crystals with 'bulky' structure. Most of the physical and chemical properties are controlled by the particle size (Attanayake et al., 2020). However, by bringing the size down to the nanometer scale, a large number of atoms on the particle surface are then less coordinated, so making the particles thermodynamically unstable. The less coordinated atoms readily chelate with ligands or surfactants (Yang et al., 2014). Among semiconductor nanocrystals, ZnS nanoparticles (NPs) are of interest due to their fascinating crystalline structures. It is well known that ZnS NPs may exist in cubic phase (zincblende) at room temperature with a bandgap of 3.68 eV, which converts to hexagonal phase (wurtzite) at higher temperatures with a bandgap of 3.77 eV (Tiwari and Dhoble., 2016). Based on the wide bandgap, ZnS NPs have the potential to be utilized in a wide range of applications in photonics, electronics, solar cells, and LEDs (Niu et al., 2014), and drug development (Ajibade et al., 2020). The latter, in particular, also relies on chelating ligands or capping agents.

Because the chelating agents are situated on the particle surface and control the chemical reactivity of the ZnS NPs, one can design the chelating ligands with functional groups that can be used to coordinate with the atoms on the surface to stabilize the ZnS NPs as well as be used for specific applications. The interesting chelating ligands are Schiff bases, which are referred to as the organic compounds containing an imine or azomethine moiety (−CH=N−). These compounds are synthesized based upon the condensation of primary amine and carbonyl compounds, such as an aldehyde or a ketone (Golcu et al., 2005; Da Silva et al., 2011; Patil et al., 2016; Bhat and Wagay, 2017), involving the replacement of the carbonyl group (C=O) of an aldehyde or ketone with an imine or azomethine moiety followed by elimination of a water molecule (Sinha et al., 2008; Md Yusof et al., 2015; Umofia et al., 2016). Schiff bases are very general and useful ligands that readily form stable complexes with most of the transition metals and hence play an important role in the development of coordination chemistry (Abdel Aziz et al., 2012). It is very interesting to note that Schiff bases exhibit strong bioactivities, such as antiviral (Sriram et al., 2006), antifungal (Zishen et al., 1993), antimalarial (Rathelot et al., 1995), antibacterial (Karthikeyan et al., 2006), antitumor (Kowol et al., 2009), and anticancer (Zishen et al., 1993; Shi et al., 2007) activities. Due to their stability, Schiff bases have a broad scope of organic and medicinal chemistry applications (Qin et al., 2013). They contain strong donor sites due to imine nitrogen atoms, and therefore, the azomethine structure has the ability to exhibit biological activities (Safari and Gandomi-Ravandi, 2014). Schiff base-related compounds, such as triapine, have potential for medicinal applications (Rejmund et al., 2018). In particular, Schiff bases containing salicylaldehyde moiety have been known to have anticancer activities (Qin et al., 2013).

It is also interesting to note that due to their simple chemical reactions, Schiff bases can be synthesized by different methods, including conventional reflux and eco-friendly or green syntheses (Ali et al., 2020). Various green synthesis methods have been introduced, including synthesis that uses water as solvent, the grinding method, microwave irradiation, and the sonication method. Green synthesis in general has been found to minimize the reaction time, but results in high efficiency.

In light of the above background, in this study two Schiff bases containing salicylaldehyde moiety were synthesized using the conventional method, where salicylaldehyde and thiosemicarbazide or 4-amino-4H-1,2,4-triazole were heated under

reflux in ethanolic solution. The compounds were isolated and purified with the recrystallization method, giving a 25–50 percentage yield. These two Schiff bases were then used for the first time to encapsulate ZnS NPs, employing the co-precipitation method, which is a rapid, simple, energy efficient, and low temperature process (Rane et al., 2018). The chemical structure of the Schiff bases and their encapsulated ZnS NPs were confirmed by the spectroscopic method. The antibacterial activities of the synthesized Schiff bases and their encapsulated ZnS NPs were screened against four different species of bacterial strains (namely *Bacillus subtilis, Escherichia coli, Pseudomonas aeruginosa,* and *Staphylococcus aureus)*, and they were compared with the standard antibiotic, streptomycin. The main objective of this study is to investigate the effect of the encapsulation of the two Schiff bases on the antibacterial activity of ZnS NPs against the four bacterial strains, and the novelty is the usage of the two Schiff bases as capping agents.

2. Methods

All the chemicals in this study were of analytical grade. They were purchased from Sigma-Aldrich or Fluka (Buchs, Switzerland) and were used as received. The IR spectra were recorded using the KBr pellet method on an FTIR spectrophotometer (Prestige-21; Shimadzu, Japan) in the range of 4500–500 cm^{-1}. The electronic spectra were determined using a UV-Visible Spectrophotometer (UV-2600; Shimadzu, Japan) with distilled water and ethanol as solvents for the Schiff bases encapsulated ZnS NPs and ligands, respectively, in the range of 200–900 cm^{-1}. The EI mass spectra were recorded on a mass spectrometer (QP2010 Ultra; Shimadzu, Japan). The photoluminescence spectra were recorded on a spectrofluorophotometer (RF-6000; Shimadzu, Japan). The scanning electron microscopic (SEM) images were measured on a SEM microscope (JSM-7610F: JEOL, Japan) with a magnification of 20,000×. Energy-dispersive X-ray spectroscopy (EDX) measurement was combined with the SEM for the samples without any coating. The elements near the surface of the Schiff bases encapsulated ZnS NPs were detected at least three different positions. The XRD pattern of Schiff-based encapsulated ZnS NPs was recorded on an X-ray diffractometer (XRD-7000, Shimadzu, Japan) with Cu Kα radiation (λ = 0.15418 nm) operating at 30 mA and 40 kV. The data were collected over a diffraction angle of 10–80°. The antibacterial activities of the Schiff bases and their encapsulated ZnS NPs were screened against *B. subtilis, E. coli, P. aeruginosa,* and *S. aureus* bacterial strains using the agar well diffusion method. All the experiments and analyses were done at Universiti Brunei Darussalam.

In the current study, two Schiff bases containing salicylaldehyde moiety (*i.e.* salicylaldehyde 2-methyl-3-thiosemicarbazone [Sal2me3TSC] and salicylaldehyde 4-amino-4H-1,2,4-triazole [SalTriazole]) were synthesized using the conventional refluxing method. The chemical structures of Sal2me3TSC and SalTriazole are shown in Figure 1. In the synthesis of Sal2me3TSC, salicylaldehyde (0.2415 g, 1.98 mmol), 2-methyl-3-thiosemicarbazide (0.2072 g, 1.97 mmol), and 50 mL methanol were mixed in a 100 mL round-bottomed flask. The pale-yellow solution was then heated under reflux, and the progress of the reaction was monitored using TLC. After refluxing for about 2 h and 30 min, the reaction was stopped, and the resulting solution was left to cool overnight. The yellow precipitate of Sal2me3TSC obtained from the reaction was filtered using gravity filtration and washed with cold methanol. The characterizations of Sal2me3TSC are as follows: Yield: 0.1692 g (41.1%). M. p 171-173°C. IR ($\upsilon_{max,}$ cm^{-1}, KBr pellet): 3431 ν(N−H), 3275 ν(O−H), 2924 ν(C-H), 1577 ν(C=N), and 1493 ν(C=S). ^{1}H NMR (DMSO-d_6, 500 MHZ, δ ppm) δ_H: 10.08 (s, 1H, phenolic proton), 8.31-8.20 (m, 2H, $-NH_2$), 8.05 (s, 1H, −CH=N), 8.03 - 6.81 (m, 4H, aromatic protons), and 3.75 (s, 3H, $-CH_3$) (Sanif, 2020). SalTriazole was synthesized by

adding salicylaldehyde (0.20 g. 1.64 mmol), 4-amino-4H-1,2,4-triazole (0.134 g, 1.64 mmol) and ethanol (20 ml) into a 50 ml of round-bottomed flask. A few drops of glacial acetic acid were added as a catalyst, and the resulting mixture was colorless when heated under reflux. The progress of the reaction was followed by TLC, and it was stopped after 8 h. After cooling to room temperature, white cotton-like precipitate was then obtained, collected by vacuum filtration, and washed with cold ethanol. The crude product of SalTriazole was then recrystallized with a mixture of hot ethanol and ethyl acetate and dried in a desiccator containing anhydrous silica. The characterizations of SalTriazole were as follows: Yield: 0.0317 g (25%); m.p. 229-231℃; IR ($\upsilon_{max,}$ cm^{-1}): 3461 υ(O–H), 2855-3030 υ(C–H), 1603 υ(C=N). ^{1}H NMR (DMSO-d_6, 500 MHZ, δ ppm) δ_H: 10.50 (br, 1H, phenolic proton), 9.28 (s, 1H, –CH=N), 9.17 (s, 2H, triazole-2H), 7.80 (d, 1H), 7.44 (t, 1H), 7.00 (d, 1H), 6.95 (t, 1H) (aromatic protons) (Ali, 2017).

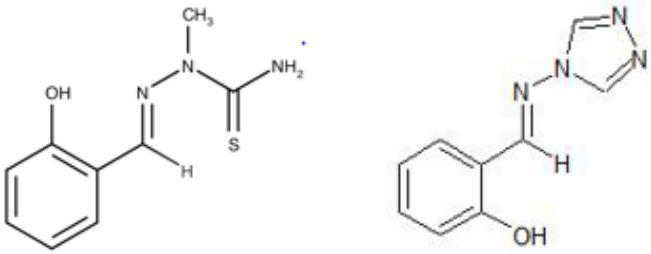

Figure 1 The chemical structures of Sal2me3TSC (left) and SalTriazole (right)

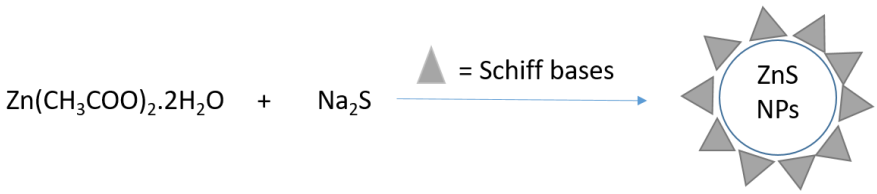

Scheme 1 The preparation of the Schiff base encapsulated ZnS NPs

The Sal2me3TSC and SalTriazole encapsulated ZnS NPs were synthesized using the co-precipitation method. The synthesis steps follow the reported procedure (Ayodhya et al., 2019). The reaction scheme is shown in Scheme 1. Zinc acetate dihydrate (0.25 M, 1.3719 g, 6.25 mmol) and sodium sulfide (0.25 M, 1.8014g, 7.50 mmol) were dissolved in 25 mL and 30 mL of ultrapure water in 125 mL conical flasks, respectively. The solutions were stirred for 30 min to create homogeneous solutions. The individual Schiff bases of Sal2me3TSC (1 mM, 0.0021 g, 0.01 mmol) and SalTriazole (1 mM, 0.0019 g, 0.01 mmol) were dissolved in 10 mL of methanol. After 30 min, the Schiff base was added into the flask containing the zinc acetate dihydrate solution. A solution of sodium sulfide was then added to the reaction mixture dropwise under constant stirring, whereby a white precipitate of ZnS NPs was immediately formed in the reaction mixture. The resulting precipitate was isolated by centrifugation and then washed several times using distilled water and ethanol to remove the unreacted chemicals. The precipitated ZnS NPs was then dried in an oven at 80°C for 5 h. The yield obtained for ZnS-Sal2me3TSC NPs was 0.7016 g; IR (υ_{max}, cm^{-1}): 3394 υ(O-H), 1625 υ(C=N), and 0.7135 g was obtained for ZnS-SalTriazole NPs; IR (υ_{max}, cm^{-1}): 3318 υ(O-H), 1632 υ(C=N).

The antibacterial screening tests of the ZnS-Sal2me3TSC NPs and ZnS-SalTriazole NPs, as well as their respective Schiff bases, were carried out using the agar well diffusion method (Bauer et al., 1966). 100 µL of the pathogenic bacteria were grown in 7 mL of nutrient broth by incubating them at 37°C in an incubator. The growth of the bacteria was

adjusted according to the 0.5 McFarland Turbidity standard, with the absorbance being 0.08–0.1 at 600 nm. 200 µL of the bacterial suspension were spread onto Mueller Hinton agar (MHA) using a sterilized glass spreader. Wells were created using a borer, equally spread out across the plate. Forty µL of the samples to be tested were pipetted into each well. Plates containing gram-positive (*S. aureus* ATCC 29213 and *B. subtilis* ATCC 1174) and gram-negative (*E. coli* ATCC 11775 and *P. aeruginosa* ATCC 27853) bacteria were incubated for 24 h at 37°C. The diameter of the inhibition zones was then measured in millimeters after the incubation process was completed. In this antibacterial test, a standard antibiotic (*i.e.,* streptomycin) was used as a positive control.

3. Results and Discussion

3.1. FTIR

Figure 2 shows the FTIR spectra of ZnS-Sal2me3TSC and ZnS-SalTriazole NPs. The spectra of Sal2me3TSC and SalTriazole are depicted for comparison. It is important to note that the marker vibrational band of the Schiff bases related to the stretching of the –CH=N– imine moiety was observed at 1578 cm^{-1}. The broad vibrational band at 3400–3600 cm^{-1} was assigned to N–H and O–H stretching vibrational modes. The weak intensity bands at 2924 and 2855 cm^{-1} were assigned to the vibrations of alkyl C–H, respectively. Upon the formation of Schiff base encapsulation ZnS NPs, the FTIR spectra are dominated by the vibrational band at 1625 and 1625 cm^{-1} for ZnS-Sal2me3TSC and ZnS-SalTriazole NPs, respectively, which were assigned to the deformation vibration of the N–H band. This spectral shift of C=N reflected the disruption of the π-electron delocalization of the ligands, which might be attributed to the coordination of the sulfur atom from the Schiff base with the Zn^{2+} ions (Zishen et al., 1993). Importantly, the spectrum of ZnS-Sal2me3TSC shows that there is a shift in the peaks of the C=N stretching of the Schiff base. The characteristic vibrations of ZnS were observed as a broad band in the range of 500–700 cm^{-1}, while the peak at around 1000 cm^{-1} was due to the resonance interaction of the ZnS lattice. The ZnS-Sal2me3TSC and ZnS-SalTriazole NPs show almost similar spectral features, where the peak intensities of the Schiff bases were covered by those of ZnS.

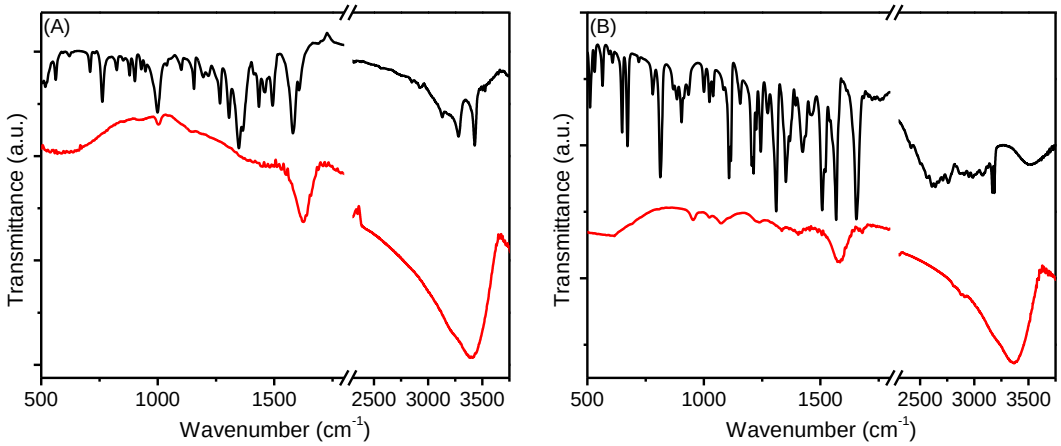

Figure 2 IR spectra of (A) Sal2me3TSC (black line) and its ZnS NPs (red line); (B) SalTriazole (black line) and its ZnS NPs (red line)

3.2. UV-Vis and PL

The UV-Vis spectra of the ZnS-Sal2me3TSC and ZnS-SalTriazole NPs also show a shift of the respective Schiff bases from 332 nm to 337 nm and from 275 nm to 322 nm, as shown in Figure 3. The spectral bands of Sal2me3TSC and SalTriazole are assigned to the π-π*

transition of the organic Schiff base compounds. The spectral shift suggests that the changes in the π-electron delocalization of the ligands occurred upon their encapsulation to the ZnS NPs. Figure 3 also shows the photoluminescence spectra of the ZnS-Sal2me3TSC and ZnS-SalTriazole NPs with their respective Schiff bases upon excitation at 332 nm.

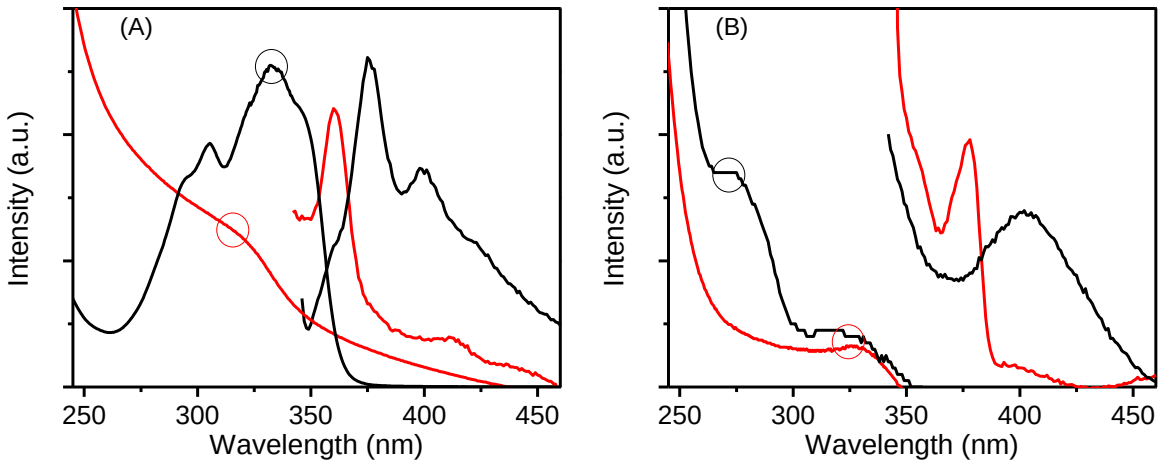

Figure 3 The UV-Visible absorption and photoluminescence spectra of (A) Sal2me3TSC (black line) and its ZnS NPs (red line), and (B) SalTriazole (black line) and its ZnS NPs (black line)

It is clearly observed that the Schiff bases, Sal2me3TSC and SalTriazole are emissive, with the fluorescence spectra being the mirror images or their respective absorption spectrum, suggesting that their fine electronic structures remain intact in the excited state. Notably, the emission of the ZnS NPs is blue shifted by about 40 nm as compared with those of the Schiff bases, and the emission intensity of the ligands was reduced due to the metal-ligand charge transfer in the ZnS-Sal2me3TSC and ZnS-SalTriazole NPs.

3.3. SEM and EDX

Figure 4 shows the SEM images of ZnS-Sal2me3TSC and ZnS-SalTriazole NPs, respectively. The SEM images suggested that the ZnS-Sal2me3TSC NPs form smaller particles as compared to the ZnS-SalTriazole NPS, where the latter was found to be a few hundred nm. Importantly, the EDX elemental analysis indicated that the ratio of Zn and S atomic percentage ratio in the ZnS-Sal2me3TSC and ZnS-SalTriazole NPs was more or less 1:1, implying that the ZnS structure remains intact. The SEM and EDX analyses confirmed the formation of ZnS NPs, which can be seen to be agglomerated in the SEM images.

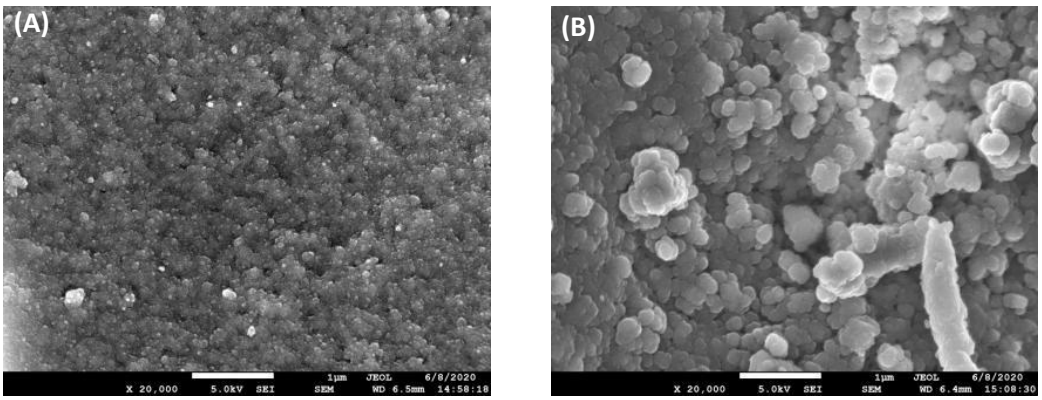

Figure 4 The SEM images of (A) ZnS-Sal2me3TSC and (B) ZnS-SalTriazole NPs

3.4. XRD Analysis

The crystalline structures of the ZnS-Sal2me3TSC and ZnS-SalTriazole NPs were confirmed by the XRD pattern. As shown in Figure 5, the set of diffraction peaks at 28.9°, 48.0°, and 56.8° were unambiguously attributed to the (111), (220), and (311) crystal planes of zincblende, in agreement with the peaks of a cubic crystal phase of ZnS (JCPDS#80-0020). The similar XRD pattern of ZnS-Sal2me3TSC and ZnS-SalTriazole NPs indicated that the crystalline structure is solely addressed to ZnS, suggesting that its crystal is unchanged upon encapsulation with Schiff bases. In other words, Schiff bases are encapsulated on the ZnS NPs, rather than inside the NPs, which might interrupt the crystalline structure of ZnS.

The broad diffraction peaks indicate that the crystallite sizes of the ZnS NPs are small. The average crystallite sizes (L) were then estimated using the Scherrer equation (Yustanti et al., 2016; Bramantyo et al., 2019).

$$L = K \cdot \lambda/(\beta \cos \theta) \quad (1)$$

where K = 0.89 is the Scherrer constant related to the shape factor of nanoparticles and λ is the X-ray wavelength. Based on the full width of the half maximum (β) of the Bragg diffraction angle 2θ at 28.9°, the average crystallite sizes of the ZnS-Sal2me3TSC and ZnS-SalTriazole NPs were calculated to be 56.2 and 60.5 nm, respectively.

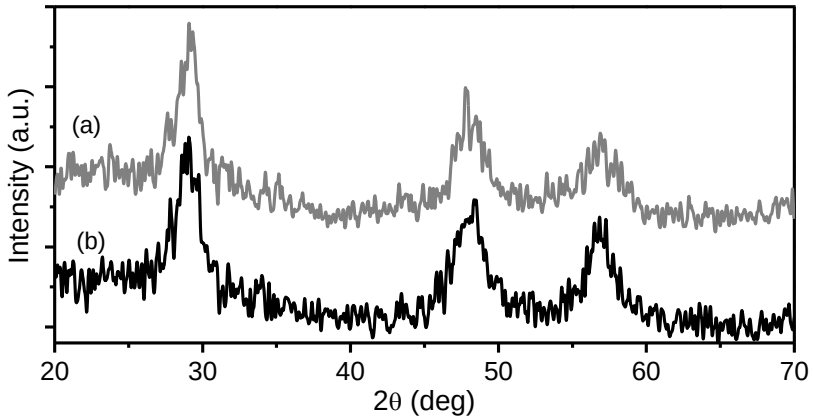

Figure 5 XRD patterns of (a) ZnS-Sal2me3TSC NPs and (b) ZnS-SalTriazole NPs

3.5. Antibacterial activity

Table 1 summarizes the antibacterial activities of ZnS-Sal2me3TSC and ZnS-SalTriazole NPs.

Table 1 The antibacterial activities of the synthesized Schiff bases and their ZnS NPs

Compound	Zone of inhibition (mm)			
	E. coli	*B. sub*	*P. aeru*	*S. aure*
Sal2me3TSC	N.D	N.D	N.D	N.D
SalTriazole	N.D	N.D	N.D	N.D
ZnS-Sal2me3TSC NPs	N.D	N.D	N.D	N.D
ZnS-SalTriazole NPs	N.D	N.D	N.D	N.D
Streptomycin	30	33	24	20

N.D = Not Detected

The antibacterial activities of Sal2me3TSC and SalTriazole Schiff bases are also listed along with the positive control, streptomycin. Both the ZnS NPs showed no inhibition of the growth of all the gram-positive and gram-negative bacterial strains in this study. Similarly,

with the same concentration, the Schiff bases were also inactive against the pathogenic bacteria. The results suggest that they did not show any antibacterial activities under the experimental conditions in this study, which may be due to their high minimum inhibition concentration. Therefore, further detailed study on the minimum inhibition and minimum bactericidal concentrations of the ZnS-Sal2me3TSC and ZnS-SalTriazole NPs and their Schiff bases is currently being pursued in our laboratory.

4. Conclusions

Two new Schiff bases of salicylaldehyde derivatives (namely ZnS-Sal2me3TSC and ZnS-SalTriazole) have been successfully synthesized using the conventional refluxing method. Their chemical structures have been confirmed by spectroscopic methods. The two Schiff bases were utilized as stabilizing agents to encapsulate ZnS NPs using the co-precipitation method. The chemical, electronic, composition, and crystal structures of ZnS-Sal2me3TSC and ZnS-SalTriazole NPs were characterized using FTIR, UV-Vis, EDX, and XRD analyses. The antibacterial studies suggested that the Schiff base ligands, as well as the ZnS-Sal2me3TSC and ZnS-SalTriazole NPs, are inactive and are most likely due to the higher minimum inhibition concentration beyond the experimental range in this current study. Overall, the results suggest the possibility of exploring ZnS NPs further in the future for their potential bioapplications, investigating Schiff bases and other bioactive ligands.

Acknowledgements

The authors would like to extend their deepest gratitude to the Chemical Sciences, Environmental and Life Sciences, Applied Physics, Geosciences of the Faculty of Science, Centre for Advanced Material and Energy Sciences (CAMES), Universiti Brunei Darussalam, and Faculty of Resource Science and Technology, Universiti Malaysia Sarawak. MHSAH is especially grateful to the Chemical Sciences for FIC Grant No. UBD/RSCH/1.4/FICBF(b)/2020/024, and YWS is grateful for grant from Universiti Brunei Darussalam (Research Grant No. UBD/RSCH/1.4/FICBF(b)/2018/019).

References

Abdel Aziz, A.A., Salem, A.N.M., Sayed, M.A., Aboaly, M.M., 2012. Synthesis, Structural Characterization, Thermal Studies, Catalytic Efficiency, and Antimicrobial Activity of Some M(II) Complexes with ONO Tridentate Schiff Base N-Salicylidene-o-Aminophenol (SaphH 2). *Journal of Molecular Structure,* Volume 1010, pp. 130–138

Ajibade, P.A., Oluwalana, A.E., Sikakane, B.M., Singh, M., 2020. Structural, Photocatalytic and Anticancer Studies of Hexadecylamine Capped ZnS Nanoparticles. *Chemical Physics Letters,* Volume 755, pp. 137813

Ali, N.H.S.O., Hamid, M.H.S.A., Putra, N.A.A.M.A., Adol, H.A., Mirza, A.H., Usman, A., Siddiquee, T.A., Hoq, M.R., Karim, M.R., 2020. Efficient Eco-Friendly Syntheses of Dithiocarbazates and Thiosemicarbazones. *Green Chem. Lett. Rev.*, Volume 13(2), pp. 129–140

Ali, N.H.S.O., 2017. Synthesis and Characterization of Some Novel Schiff Bases from Amino Derivatives and Aldehydes/Ketones. *Master Thesis*, UBD

Attanayake, S., Okuya, M., Murakami, K., 2020. Spray Angle Dependence for the Growth of Terrace-Truncated Nanocone Structure of Gallium-doped Zinc Oxide by Advanced Spray Pyrolysis Deposition Technique. *International Journal of Technology,* Volume 11(1), pp. 81–90

Ayodhya, D., Veerabadham, G., 2019. Fabrication of Schiff Base Coordinated ZnS Nanoparticles for Enhanced Photocatalytic Degradation of Chlorpyrifos Pesticide and Detection of Heavy Metal Ions*, J. Materiomics,* Volume 5(3), pp. 446–454

Ayodhya, D., Venkatesham, M., Kumari, A.S., Mangatayaru, K.G., Veerabadham, G., 2013. Synthesis, Characterization of ZnS Nanoparticles by Coprecipitation Method using Various Capping Agents—Photocatalytic Activity and Kinetic Study*. Journal of Applied Chemistry*, Volume 6(1), pp. 1–9

Bauer, A.W., Kirby, W.M.M., Sherris, J.C., Turck, M., 1966. Antibiotic Susceptibility Testing by a Standardized Single Disk Method. *American Journal of Clinical Pathology,* Volume 45(4), pp. 493–496

Bhat, A.R., Wagay, M.H., 2017. Synthesis of Schiff's Base Derivatives using Water as Solvent. (A Green Methodology). *International Journal for Research in Applied Science & Engineering Technology*, Volume 5(11), pp. 971–982

Bramantyo, A., Murakami, K., Okuya, M., Udhiarto, A., Poespawati, N.R., 2019. Morphological and Structural Study of Vertically Aligned Zinc Oxide Nanorods Grown on Spin Coated Seed Layers. *International Journal of Technology,* Volume 10(1), pp. 147–158

Carrillo-Carrión, C., 0árdenas, S., Simonet, B.M., Valcárcel, M., 2009. Quantum Dots Luminescence Enhancement due to Illumination with UV/Vis Light. *Chemical Communicatio,* Volume 35, pp. 5214–5226

Da Silva, C.M., Da Silva, D.L., Modolo, L.V., Alves, R.B., De Resende, M.A., Martins, C.V.B., De Fátima, Â., 2011. Schiff Bases: A Short Review of Their Antimicrobial Activities. *Journal of Advanced Research,* Volume 2(1), pp. 1–8

Golcu, A., Tumer, M., Demirelli, H., Wheatley, R.A., 2005. Cd(II) and Cu(II) Complexes of Polydentate Schiff Base Ligands: Synthesis, Characterization, Properties and Biological Activity. *Inorganica Chimica Acta,* Volume 358(6), pp. 1785–1797

Karthikeyan, M.S., Prasad, D.J., Poojary, B., Subrahmanya Bhat, K., Holla, B.S., Kumari, N.S., 2006. Synthesis and Biological Activity of Schiff and Mannich Bases Bearing 2,4-Dichloro-5-Fluorophenyl Moiety*. Bioorg. Med. Chem*, Volume 14(22), pp. 7482–7489

Keskin, I.C., Türemiş, M., Katı, M.I., Kibar, R., Çetin, A., 2019. Effects of CdS Quantum Dot in Polymer nanocomposite: In Terms of Luminescence, Optic, and Thermal Results, *Radiation Physics and Chemistry,* Volume 156(3), pp. 137–143

Kowol, C.R., Trondl, R., Heffeter, P., Arion, V.B., Jakupec, M.A., Roller, A., Galanski, M., Berger, W., Keppler, B.K., 2009. Impact of Metal Coordination on Cytotoxicity of 3-Aminopyridine-2- Carboxaldehyde Thiosemicarbazone (Triapine) and Novel Insights into Terminal Dimethylation*. J. Med. Chem*. Volume 52(16), pp. 5032–5043

Mansur, H.S., 2010. Quantum Dots and Nanocomposites. *Wiley Interdiscip. Rev. Nanomed. Nanobiotechnol*, Volume 2, pp. 113–129

Mansur, H.S., Vasconcelos, W.L., Grieser, F., Caruso, F., 1999. Photoelectrochemical Behaviour of CdS "Q-State" Semiconductor Particles in 10,12-Nonacosadiynoic Acid Polymer Langmuir-Blodgett Films. *Journal of Materials Science,* Volume 34, pp. 5285–5291

Md Yusof, E.N., Ravoof, T.B.S.A., Tiekink, E.R.T., Veerakumarasivam, A., Crouse, K.A., Tahir, M.I.M., Ahmad, H., 2015. Synthesis, Characterization and Biological Evaluation of Transition Metal Complexes Derived from N, S Bidentate Ligands. *Int. J. Mol. Sci*., Volume 16(5), pp. 11034–11054

Niu, G., Li, N., Wang, L., Li, W., Qiu, Y., 2014. Combined Post-Modification of Iodide Ligands and Wide Band Gap ZnS in Quantum Dot Sensitized Solar Cells. *Phys. Chem. Chem. Phys.*, Volume 16(34), pp. 18327–18332

Patil, C.J., Patil, M.C., Patil, M.C., Mahale, R.G., 2016. Studies on Schiff Bases from Methyl-1-Naphthyl Ketone. Part-I: Synthesis and Characterization of Ketimines from 1-Acetylnaphthalene with Derivatives of Aniline*. Der Pharma Chem*, Volume 8(1), pp. 99–103

Qin, W., Long, S., Panunzio, M., Biondi, S., 2013. Schiff Bases: A Short Survey on an Evergreen Chemistry Tool. *Molecules,* Volume 18(10), pp. 12264–12289

Rane, A.V., Kanny, K., Abitha, V.K., Thomas, S., 2018. *Methods for Synthesis of Nanoparticles and Fabrication of Nanocomposites, in Bhagyaraj, S.M., Oluwafemi, O.S., Kalarikkal, N., Thomas, S. (Eds.) Synthesis of Inorganic Nanomaterials*. Woodhead Publishing, Chapter 5, pp. 121–139

Rathelot, P., Vanelle, P., Gasquet, M., Delmas, F., Crozet, M.P., Timon-David, P., Maldonado, J., 1995. Synthesis of Novel Functionalized 5-Nitroisoquinolines and Evaluation of in vitro Antimalarial Activity. *European Journal of Medicinal Chemistry*, Volume 30(6), pp. 503–508

Rejmund, M., Mrozek-Wilczkiewicz, A., Malarz, K., Pyrkosz-Bulska, M., Gajcy, K., Sajewicz, M., Musiol, R., Polanski, J., 2018. Piperazinyl Fragment Improves Anticancer Activity of Triapine. *PLoS ON,* Volume 13(4), pp. 1–25

Safari, J., Gandomi-Ravandi, S., 2014. Structure, Synthesis and Application of Azines: A Historical Perspective. *RSC Adv.,* Volume 4, pp. 46224–46249

Sanif, M.N.M.N.M., 2020. Synthesis and Fabrication of Schiff Base Coordinated ZnS and CdS Nanoparticles, *FYP Thesis*, UBD

Shi, L., Ge, H.M., Tan, S.H., Li, H.Q., Song, Y.C., Zhu, H.L., Tan, R.X., 2007. Synthesis and Antimicrobial Activities of Schiff Bases Derived from 5-Chloro-Salicylaldehyde. *European Journal of Medicinal Chemistry*, Volume 42(4), pp. 558–564

Sinha, D., Tiwari, A.K., Singh, S., Shukla, G., Mishra, P., Chandra, H., Mishra, A.K., 2008. Synthesis, Characterization and Biological Activity of Schiff Base Analogues of Indole-3-Carboxaldehyde. *Eur. J. Med. Chem.*, Volume 43(1), pp. 160–165

Sriram, D., Yogeeswari, P., Myneedu, N.S., Saraswat, V., 2006. Abacavir Prodrugs: Microwave-Assisted Synthesis and Their Evaluation of Anti-HIV Activities. *Bioorg. Med. Chem. Lett*. Volume 16(8), pp. 2127–2129

Tiwari, A., Dhoble, S.J., 2016. Stabilization of ZnS Nanoparticles by Polymeric Matrices: Syntheses, Optical Properties and Recent Applications*. RSC Adv.*, Volume 6, pp. 64400–64420

Umofia, E., Omuaru, V.O.T., Achugasim, O., 2016. Green Solvents for the Synthesis of Some Toluidine-Derived Schiff Bases*. J. Chem. Soc. Niger*., Volume 41(1), pp. 1–10

Wei, W., Liu, C., Liu, J., Liu, X., Zou, L., Cai, S., Shi, H., Cao, Y.C., 2016. Do the Cations in Clay and the Polymer Matrix Affect Quantum Dot Fluorescent Properties*? Luminescence*, Volume 31(4), pp. 1020–1024

Yang, Y., Li, M., Xie, Y., Song, X., Qu, X., Zhao. H., 2014. Fabrication of CdS Nanoparticles on the Edges of Reduced Graphene Oxide Sheets with P2VP Polymer Brushes. *Materials Letters,* Volume 118(3), pp. 184–187

Yustanti, E., Hafizah, M.A.E., Manaf, A., 2016. Exploring the Effect of Particle Concentration and Irradiation Time in the Synthesis of Barium Strontium Titanate (BST) Ba(1-X) SrxTiO3 (X:0-1) Nanoparticles by High Power Ultrasonic Irradiation. *International Journal of Technology,* Volume 7(6), pp. 1016–1025

Zishen, W., Zhiping, L., Zhenhuan, Y., 1993. Synthesis, Characterization and Antifungal Activity of Glycylglycine Schiff Base Complexes of 3d Transition Metal Ions. *Transition Metal Chemistry*, Volume 18, pp. 291–294